Available online at www.sciencedirect.com

ScienceDirect

IFAC PapersOnline CONFERENCE PAPER ARCHIVE

IFAC PapersOnLine 56-2 (2023) 10965–10970

Impact and Abrasion Power Modeling of a Tumbling Mill for Control Design

H. Ventura-Hinostroza * **J. Sotomayor-Moriano** *
J. Oliva-Moncunill **

* *Engineering Department, Pontificia Universidad Católica del Perú, Av. Universitaria 1801, San Miguel, Lima 15088, Perú (e-mail: {hventura, jsotom}@pucp.edu.pe).*
** *Departament d'Enginyeria Minera, Industrial i TIC, Universitat Politècnica de Catalunya, Barcelona Tech, Manresa, 08242 Barcelona, Spain; (e-mail: josep.oliva@upc.edu)*

Abstract: In this research, the model of the net power draw of a tumbling mill is proposed, which is described considering the contribution of the impact power and the abrasion power separately. Nowadays, in phenomenological models used in mill control design, the net power draw in the grinding of the mineral is not described by a dynamic representation (but by experimental formulation); therefore, the validity of the model thus obtained is restricted to a given operating condition. The proposed model describes the dynamics of the impact power and the abrasion power through variables and parameters that depend on the operating conditions, therefore this model is obtained for a whole range of operation, also it is represented in the state space, which will facilitate the control design task of the milling process. Finally, simulation tests were carried out for a tumbling mill using the proposed approach.

Keywords: mathematical model, impact power, milling process, grinding media, tumbling mill

1. INTRODUCTION

The net power draw to produce a certain distribution of particles in a tumbling mill has its bases in the work developed by (Bond, 1961) in which it is display the net power draw to carry a feed of size F_{80} to a product P_{80}. An alternative taking into account the geometric variations and the change in the grinding environment is proposed by (Hogg and Fuerstenau, 1972). Important contributions are made to relate the breakage kinetics or selection function to the net power draw in ball mills (Herbst and Fuerstenau, 1980). A more detailed description of the net power draw and its relationship with the load of the mill can be seen in (Morrell, 1996), who determines that the friction forces inside the mill depend on its load and the mill rotation speed, an approach that the allows to obtain the energy absorbed by the load in the form of potential and kinetic energy. Later, (Morrell, 2004) will use this power description to relate it to the fracture function and fracture kinetics, this model can be used as an independent design tool, to extend from pilot data and optimize existing circuits, but it cannot be used for control design as real-time updating of operating point changes is not possible. (Yuwen et al., 2020) describes the net power draw, specifically the impact power, which will later be related to the breakage function that (le Roux et al., 2013) had previously developed. This model is suitable for control, but its relationship with the breakage function and breakage kinetics is reduced only to three particles distributions which may not be satisfactory for product quality issues. There are also models that deal directly with the impact power instead of the net power draw, (Jayasundara and Zhu, 2022), which are based on discrete element method (DEM). These models find their greatest utility in mill design and lose relevance for control design (Salcedo Hernandez et al., 2018) due to the computational load they represent.

In this research, the modeling of energy consumption is carried out using the Lagrange-Euler method, to formulate the dynamics of the tumbling mill, which has functional parts such as the drum, bucket, unloading lifters and kidney that are dynamically interlocked by rotational speed, friction forces, and viscosity. The proposed model considered the geometry of the mill, the variables and the operating condition to determine the impact power and the abrasion power separately.

This work is organized as follows, Section 2 deals with the modeling of a tumbling mill, Section 3 offers the results and evaluation and the Section 4 displays the conclusions.

2. TUMBLING MILL MODELING

2.1 General Formulation

To obtain the mathematical model of the tumbling mill, the Lagrangian formulation based on total energy is used:

$$L = L(q_j, \dot{q}_j) = V(q_j, \dot{q}_j) - U(q_j) = \sum_{k=1}^{n} V_k(q_j, \dot{q}_j) - \sum_{k=1}^{n} U_k(q_j) \quad (1)$$

$$\tau_L - \tau_B - \tau_\eta = \frac{d}{dt}\frac{\partial L}{\partial \dot{q}_j} - \frac{\partial L}{\partial q_j} \quad (2)$$

where:
L is the Lagrangian function,

10.1016/j.ifacol.2023.10.791

V is the total kinetic energy of the tumbling mill,
V_k is the kinetic energy of some of the functional parts of the mill (drum, bucket, unloading lifters and kidney) $k, \forall\, k\epsilon\{1 \dots n\}$, $n = 4$,
U is the total potential energy of the tumbling mill,
U_k is the potential energy of some of the functional parts of the mill $k, \forall\, k\epsilon\{1 \dots n\}$, $n = 4$,
q_j are the generalized coordinates $j, \forall\, j\epsilon\{1, 2\}$,
τ_L is the total torque of the tumbling mill,
τ_B is the torque due to air friction forces,
τ_η is the torque due to frictional forces in the kidney.

To develop the modeling of the tumbling mill, Fig. 1 and Table 1 are considered.

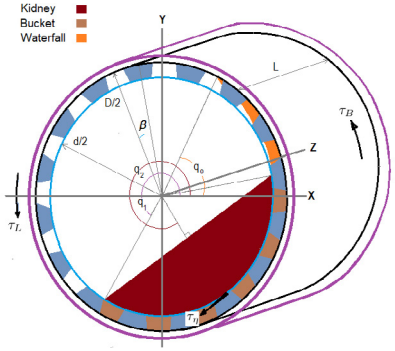

Fig. 1. Structural representation of a tumbling mill.

Table 1. Values of the parameters of a tumbling mill.

Symbol	Description	Units
D_e	Mill outside diameter	m
D	Mill top inside diameter	m
d	Mill inside diameter	m
d_p	Mill pitch diameter	m
L	Mill inside length	m
V_l	Lifter load volume	m^3
β	Mean angle of separation between lifters	rad
m_t	Mill drum mass	kg
J_t	Mill drum moment of inertia	kg
q	Drum general angle	rad
q_1	Bucket start angle	rad
q_2	Kidney position angle	rad
q_o	Unloading lifters angle	rad
n_g	Number of loaders in the bucket	
n_c	Number of unloading lifters	
m_g	Total mass on bucket	kg
m_{c_i}	Mass on lifters unloader i	kg
m_r	Total kidney mass	kg
ρ_g	Density of the material present in the bucket	kg/m^3
ρ_r	Density of the material present in the kidney	kg/m^3
η	Apparent viscosity in the kidney	$N.s/m^2$
ε_c	Kidney shear stress (bottom)	N/m^2
$\dot{W}_I$	Impact power	W
$\dot{W}_A$	Abrasion power	W

2.2 Drum Energy Equations

From Fig. 1 the trigonometric relations are deduced to determine the coordinates of the center of mass of the mill drum with respect to the reference axes XYZ:

$$\mathbf{c_t} = (x_t, y_t, z_t) = \left(0, 0, \frac{L}{2}\right) \tag{3}$$

Then the kinetic energy and potential energy of the mill drum are obtained,

$$V_t = \frac{1}{2} J_t \dot{q}^2 \tag{4}$$

$$U_t = 0 \tag{5}$$

In addition the moment of inertia is

$$J_t = \frac{1}{2} m_t \left(\frac{D_e^2}{4} + \frac{d_p^2}{4}\right) \qquad d_p = \frac{D + d}{2} \tag{6}$$

2.3 Bucket Energy Equations

From Fig. 1, the trigonometric relationships are deduced to determine the coordinates of the center of mass in any component i of loaders in the bucket in (7), the kinetic energy is in (8), and potential energy is in (9),

$$\mathbf{c_{g_i}} = (x_{g_i}, y_{g_i}, z_{g_i}) = \left(\frac{d_p}{2}\cos(q_1 + \dot{q}t + 2\beta i), \frac{d_p}{2}\sin(q_1 + \dot{q}t + 2\beta i), \frac{L}{2}\right) \tag{7}$$

$$V_{g_i} = \frac{1}{2} m_{g_i} \left(\dot{x}_{g_i}^2 + \dot{y}_{g_i}^2 + \dot{z}_{g_i}^2\right) = \frac{1}{8} m_{g_i} d_p^2 \dot{q}^2 \tag{8}$$

$$U_{g_i} = m_{g_i} g \frac{d_p}{2} \sin(q_1 + \dot{q}t + 2\beta i) \approx m_{g_i} g \frac{d_p}{2} \sin(q_1 + 2\beta i) \tag{9}$$

Also it can be seen that the total mass on bucket m_g, colored brown, is in (10), and the number of loaders in the bucket is in (11).

$$m_g = \rho_g V_l \left(\frac{q_2 - q_1}{\beta}\right) = \sum_{i=1}^{n_g} m_{g_i} \tag{10}$$

$$n_g = \left\| \frac{q_2 - q_1}{\beta} \right\| \tag{11}$$

To obtain the total kinetic energy and potential energy of the loaders in the bucket, the sums of the n_g components are obtained,

$$V_g = \sum_{i=1}^{n_g} V_{g_i} = \frac{1}{8} d_p^2 m_g \dot{q}^2 \tag{12}$$

$$U_g = \sum_{i=1}^{n_g} U_{g_i} = \sum_{i=1}^{n_g} g m_g \left(\frac{1}{n_g}\right) \frac{d_p}{2} \sin(q_1 + 2\beta i) \tag{13}$$

To make it continuous, here it is postulated that there is a diameter d_e ($d_e < D$) in which the mass m_g remains the same. If dm_g is a mass differential (14), integrating from q_1 to $(2q_2 - q_1)$ as shown in (15), and isolating d_e (16) is obtained,

$$dm_g = \rho_g L \left(\pi \left(\frac{d_e^2}{2}\right)^2 \frac{d\theta}{2\pi} - \pi \left(\frac{d^2}{2}\right)^2 \frac{d\theta}{2\pi}\right) \tag{14}$$

$$m_g = \int_{q_1}^{2q_2 - q_1} dm_g = \rho_g V_l \left(\frac{q_2 - q_1}{\beta}\right) \tag{15}$$

$$d_e = \sqrt{\frac{4V_l}{L\beta} + d^2} \tag{16}$$

Consequently, the mass m_g is also expressed continuous in terms of the diameter d_e:

$$m_g = \rho_g L \left(\frac{d_e^2 - d^2}{4}\right)(q_2 - q_1) \tag{17}$$

then the potential energy in (13) is updated:

$$U_g = \int_{q_1}^{2q_2-q_1} g\rho_g L\left(\frac{d_e+d}{4}\right)\left(\frac{d_e^2-d^2}{8}\right)\sin(\theta)d\theta$$
$$= g\rho_g L\left(\frac{d_e+d}{4}\right)\left(\frac{d_e^2-d^2}{8}\right)(cos(q_2-\alpha)-cos(q_2+\alpha)) \quad (18)$$

where: $\alpha = q_2 - q_1$

2.4 Unloading Lifters Energy Equations

From Fig. 1 the trigonometric relationships are acquired to define the coordinates of the center of mass of any component i of the lifter's unloader with respect to the reference axes:

$$\mathbf{c_{c_i}} = (x_{c_i}, y_{c_i}, z_{c_i}) = \left(\frac{d_p}{2}\cos(q_1+2\alpha+\dot{q}t+2\beta i), \frac{d_p}{2}\sin(q_1+2\alpha+\dot{q}t+2\beta i), \frac{L}{2}\right) \quad (19)$$

The lifter's unloader are shown in orange in Fig. 1, their quantity is n_c and is determined by:

$$n_c(2\beta) = 2\pi + q_o - (q_2 + (q_2 - q_1)) \quad (20)$$

The angle q_o is determined by the centripetal force expressed as:

$$m_{c_{n_c}} g\sin(q_o) = m_{c_{n_c}} \frac{(\frac{d}{2})^2\dot{q}^2}{\frac{d}{2}}$$
$$q_o = \arcsin\left(\frac{\frac{d}{2}\dot{q}^2}{g}\right) \quad (21)$$

Substituting (21) into (20) leads to:

$$n_c = \left\| \frac{2\pi + \arcsin\left(\frac{d}{2g}\dot{q}^2\right) - (q_2 + (q_2 - q_1))}{2\beta} \right\| \quad (22)$$

Fig. 1 shows that the total mass of lifter's unloader m_c , colored orange, is

$$m_c = \rho_g V_l \left(\frac{2\pi + q_o - (q_2+\alpha)}{2\beta}\right) = \sum_{i=1}^{n_c} m_{c_i} \quad (23)$$

To find the total kinetic energy and potential energy of the unloading lifters, the same operations are carried out as those performed for the bucket. As a result it is get:

$$V_c = \frac{1}{8} d_p^2 m_c \dot{q}^2 \quad (24)$$
$$U_c = g\rho_g L\left(\frac{d_e+d}{4}\right)\left(\frac{d_e^2-d^2}{8}\right)(cos(q_2+\alpha)-cos(2\pi+q_o)) \quad (25)$$

2.5 Energy Equations of the Kidney

From Fig. 1 using trigonometric relations the kidney center of mass with respect to the axes is obtained,

$$\mathbf{c_r} = (x_r, y_r, z_r) = \left(d\frac{\sin(2q_2-q_1)-\sin(q_1)-\cos(q_2)\sin(2(q_2-q_1))\cos(q_2-q_1)}{3(2(q_2-q_1)-\sin(2(q_2-q_1)))}, d\frac{-\cos(2q_2-q_1)+\cos(q_1)-\sin(q_2)\sin(2(q_2-q_1))\cos(q_2-q_1)}{3(2(q_2-q_1)-\sin(2(q_2-q_1)))}, \frac{L}{2}\right) \quad (26)$$

The distance from the origin of XYZ to the kidney center of mass, (R_r), is obtained by applying the Pythagorean theorem:

$$R_r = \frac{d\sqrt{2-2\cos(2(q_2-q_1))+\sin^2(2(q_2-q_1))(\cos^2(q_2-q_1)-2)}}{3(2(q_2-q_1)-\sin(2(q_2-q_1)))} \quad (27)$$

The kidney mass m_r is

$$m_r = \rho_r L\frac{d^2}{8}(2(q_2-q_1)-\sin(2(q_2-q_1))) \quad (28)$$

The kinetic and potential energy of the kidney are respectively:

$$V_r = \frac{1}{2} m_r R_r^2 \dot{q}_2^2 \quad (29)$$
$$U_r = m_r g R_r \sin(q_2) \quad (30)$$

It should be noted that inside the kidney there is circulation of grinding media and slurry due to the effect of frictional forces and since this is a non-conservative force, it will be considered in τ_η of the external part in (2).

2.6 Mill Torque Equations

The Lagrangian of the mill is obtained remplacing (4), (5), (12), (18), (24), (25), (29) and (30) in (1):

$$L(q_j,\dot{q}_j) = \frac{1}{2}J_t\dot{q}^2 + \frac{1}{8}d_p^2 m_g\dot{q}^2 + \frac{1}{8}d_p^2 m_c\dot{q}^2 + \frac{1}{2}m_r R_r^2\dot{q}_2^2 - g\rho_g L\left(\frac{d_e+d}{4}\right)\left(\frac{d_e^2-d^2}{8}\right)(cos(q_2-\alpha)-cos(q_2+\alpha)) - g\rho_g L\left(\frac{d_e+d}{4}\right)\left(\frac{d_e^2-d^2}{8}\right)(cos(q_2+\alpha)-cos(2\pi+q_o)) - m_r g R_r\sin(q_2) \quad (31)$$

To determine the torques in (2), (31) is derived with respect to q and q_2, respectively:

$$\tau_L - \tau_B - \tau_\eta = \frac{d}{dt}\frac{\partial L}{\partial\dot{q}} - \frac{\partial L}{\partial q} = \ddot{q}\left(J_t + \frac{1}{4}d_p^2(m_g+m_c) + \frac{\rho_g V_l d_p^2 s_{q_o}}{4\beta\sqrt{1-s_{q_o}^2}}\right) + \dot{q}\left(\frac{1}{4}d_p^2\dot{m}_g\right) \quad (32)$$

$$\tau_\eta = \frac{d}{dt}\frac{\partial L}{\partial\dot{q}_2} - \frac{\partial L}{\partial q_2} = \ddot{q}_2\left(m_r R_r^2\right) + \dot{q}_2\left(\frac{\dot{q}_2}{2}(m_{dr}R_r^2 + 2m_r R_{dr}R_r)\right) + g(m_{dr}R_r + m_r R_{dr})\sin(q_2) + g m_r R_r\cos(q_2) \quad (33)$$

where:

$$s_{q_o} = \frac{\frac{d}{2}\dot{q}^2}{g} \quad (34)$$
$$m_{dr} = \frac{dm_r}{dq_2} = m_r\frac{2-2\cos(2(q_2-q_1))}{2(q_2-q_1)-\sin(2(q_2-q_1))} \quad (35)$$
$$R_{dr} = \frac{dR_r}{dq_2} \quad (36)$$
$$= R_r\left(\frac{4\sin(2\alpha)+2\sin(4\alpha)(\cos^2\alpha-2)-\sin^3(2\alpha)}{2(2-2\cos(2\alpha)+\sin^2(2\alpha)(\cos^2\alpha-2))} - \frac{2-2\cos(2\alpha)}{2\alpha-\sin(2\alpha)}\right)$$

The torque τ_η, is obtained from the shear stress that exists between the layers of the arc c_0 and c_1, (see Fig. 2), in this case to facilitate the calculation it will be done between the layers of arc c_0 and c_2. The speed profile of these layers is modeled with a parabolic function (also could be lineal or others):

$$(v(R)-\dot{q}_2R_r)^2 = k(R-R_r) = \frac{\left(\dot{q}\frac{d}{2}-\dot{q}_2R_r\right)^2}{\frac{d}{2}-R_r}(R-R_r)$$
$$v_R = v(R) = \dot{q}_2R_r + \left(\dot{q}\frac{d}{2}-\dot{q}_2R_r\right)\sqrt{\frac{(R-R_r)}{\frac{d}{2}-R_r}} \quad (37)$$

where $v(R)$ represents the tangential speed at a distance R from the origin of coordinates, and k is the constant that fits the values $\dot{q}$ and $\dot{q}_2$.

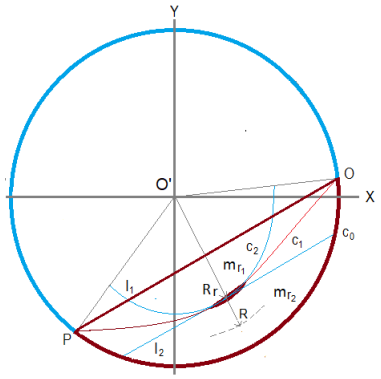

Fig. 2. Friction layers inside the kidney in the mill.

The derivative of (37) with respect to R is

$$\frac{dv(R)}{dR} = \frac{\dot{q}\frac{d}{2} - \dot{q}_2 R_r}{2\sqrt{(\frac{d}{2} - R_r)(R - R_r)}} \tag{38}$$

and evaluating it for $\frac{d}{2}$ (see Fig. 1)

$$\frac{dv(\frac{d}{2})}{dR} = \frac{\dot{q}\frac{d}{2} - \dot{q}_2 R_r}{2(\frac{d}{2} - R_r)} \tag{39}$$

The shear stress is defined as the net tangential force F_T that takes place on the surface A_T and this is proportional to the derivative of the speed with respect to the distance on the arc c_0:

$$\varepsilon_c = \frac{F_T}{A_T} = \eta \frac{dv(\frac{d}{2})}{dR} \tag{40}$$

By substituting (39) in (40) it is obtained,

$$\frac{\frac{\tau_\eta}{\frac{d}{2}} - F_\mu}{A_T} = \eta \frac{\dot{q}\frac{d}{2} - \dot{q}_2 R_r}{2(\frac{d}{2} - R_r)} \tag{41}$$

where F_μ, is the friction force exerted by the mass m_{r_1} on the mass m_{r_2}:

$$F_\mu = \mu m_{r_1} g(-\sin(q_2)) \tag{42}$$

A_T is the contact surface of the mass m_{r_2} with the tangential force,

$$A_T = 2(\alpha)\frac{d}{2}L \tag{43}$$

Substituting (42) and (43) in (41) it is obtained,

$$\tau_\eta = \frac{\eta\alpha\left(\frac{d}{2}\right)^3 L}{\frac{d}{2} - R_r}\dot{q} - \frac{\eta\alpha\left(\frac{d}{2}\right)^2 R_r L}{\frac{d}{2} - R_r}\dot{q}_2 + \mu m_{r_1} g\frac{d}{2}(-\sin(q_2)) \tag{44}$$

On the other hand τ_B is

$$\tau_B = B_t \dot{q} \tag{45}$$

where B_t is drum friction coefficient.

Substituting (44) and (45) into (32) and (33), respectively (46) and (47) are obtained,

$$\tau_L = \ddot{q}\left(J_t + \frac{1}{4}d_p^2(m_g + m_c) + \frac{\rho_g V_l d_p^2 s_{q_o}}{4\beta\sqrt{1 - s_{q_o}^2}}\right) + \dot{q}\left(B_t + \frac{1}{4}d_p^2\dot{m}_g + \frac{\eta\alpha\left(\frac{d}{2}\right)^3 L}{\frac{d}{2} - R_r}\right) - \frac{\eta\alpha\left(\frac{d}{2}\right)^2 R_r L}{\frac{d}{2} - R_r}\dot{q}_2 + \mu m_{r_1} g\frac{d}{2}(-\sin(q_2)) \tag{46}$$

$$\frac{\eta\alpha\left(\frac{d}{2}\right)^3 L}{\frac{d}{2} - R_r}\dot{q} = \ddot{q}_2\left(m_r R_r^2\right) + \dot{q}_2\left(\frac{\dot{q}_2}{2}(m_{dr}R_r^2 + 2m_r R_{dr} R_r) + \frac{\eta\alpha\left(\frac{d}{2}\right)^2 R_r L}{\frac{d}{2} - R_r}\right) + g(m_{dr}R_r + m_r R_{dr})\sin(q_2) + g m_r R_r \cos(q_2) - \mu m_{r_1} g\frac{d}{2}(-\sin(q_2)) \tag{47}$$

2.7 Equations of the Impact Power on the Kidney

The impact power differential $d\dot{W}_I$, with which the mass flow $\dot{m}_R$ impacts on the kidney is obtained as:

$$d\dot{W}_I = \dot{m}_R\left(\frac{1}{2}v_B^2 - \frac{1}{2}v_O^2\right) = -\dot{m}_R g(h_B - h_O) \tag{48}$$

and, Fig. 3 shows the parabolic path that it takes,

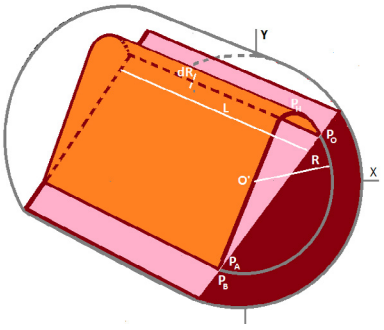

Fig. 3. Path of the waterfall in the mill.

which is given by:

$$\boldsymbol{r} = (x_o - R\dot{q}\sin(q_o)t)\,\hat{i} + \left(y_o + R\dot{q}\cos(q_o)t - g\frac{t^2}{2}\right)\hat{j} \tag{49}$$

and the speed is the following

$$\frac{d\boldsymbol{r}}{dt} = (-R\dot{q}\sin(q_o))\,\hat{i} + (R\dot{q}\cos(q_o) - gt)\,\hat{j} \tag{50}$$

Eliminating t in (49) the (51) it is obtained,

$$y - y_o = -\frac{g}{2(\frac{d}{2})^2\dot{q}^2\sin^2(q_o)}(x - x_o)^2 - \cot(q_o)(x - x_o) \tag{51}$$

The unloading position of the lifters, starts in P_O, where the position is

$$\boldsymbol{r}_O = x_o\hat{i} + y_o\hat{j} = R\cos(q_o)\hat{i} + R\sin(q_o)\hat{j} \tag{52}$$

and ends in P_B which is in the circumference (see Fig. 3):

$$y^2 + x^2 = R^2 \tag{53}$$

The position of point P_B is obtained in (54) by the intersection between the parabola (51), and the circumference (53), the time it takes to reach the kidney is in (55), the position angular is in (56), and the speed is in (57), here (21) was used,

$$\boldsymbol{r}_B = \left(x_o - 4R\sin^2(q_o)\cos(q_o)\right)\hat{i} + \left(y_o - 4R\cos^2(q_o)\sin(q_o)\right)\hat{j} \tag{54}$$

$$t_B = \frac{2\sin(2q_o)}{\dot{q}} \tag{55}$$

$$\cos(q_B) = \frac{R\cos(q_o) - 4R\sin^2(q_o)\cos(q_o)}{R} \Rightarrow q_B = 2\pi - 3q_o \tag{56}$$

$$v_B = R\dot{q}\sqrt{1 + 8\cos^2(q_o)} \tag{57}$$

The horizontal distance of $\boldsymbol{r}_B\hat{i}$ is obtained using (54) and (21),

$$\boldsymbol{r}_B\hat{i} = \frac{g}{\dot{q}^2}\sin(q_o)\cos(q_o) - 4\frac{g}{\dot{q}^2}\sin^3(q_o)\cos(q_o) \tag{58}$$

deriving it with respect to q_o and set it equal to zero

$$sin(q_o) = \sqrt{0.0785} \tag{59}$$

Substituting (59) in (21) the minimum radius that can be formed in the cataract is (Yuwen et al., 2020).

$$R_{min} = \frac{g\sqrt{0.0785}}{\dot{q}^2} \tag{60}$$

On the other hand, here it was mentioned that the center of gravity of the kidney is the distance R_r from the center of the mill, consequently the R_{min} obtained in (60) is updated to:

$$R_{min} = \begin{cases} \frac{d_e}{2} & if \;\; R_{min} \geq \frac{d_e}{2} \\ \frac{g\sqrt{0.0785}}{\dot{q}^2} & if \;\; R_r < R_{min} < \frac{d_e}{2} \\ R_r & if \;\; R_{min} \leq R_r \end{cases} \tag{61}$$

The impact of grinding media can occur in the kidney, in the best of cases, and/or in the lining of the lifters, in the worst of cases. To maximize the impact the following condition must be true,

$$q_{toe} = q_1 = q_2 - \alpha = q_B \tag{62}$$

where the toe angle q_{toe} of the kidney is equal to the angular position q_B where the grinding media falls, avoiding falling into the liners.

To determine the impact power on the kidney (21) must be updated for a general radius R:

$$v^2(q_o) = Rg\sin(q_o) \tag{63}$$

At the point P_O it is true that $v(R) = v(q_o)$ consequently equaling (37) and (63) it is obtained

$$\sin(q_o) = \frac{1}{Rg}\left(\dot{q}_2 R_r + \left(\dot{q}\frac{d}{2} - \dot{q}_2 R_r\right)\sqrt{\frac{R - R_r}{\frac{d}{2} - R_r}}\right)^2 \tag{64}$$

In (48) it is observed that the heights h_B and h_O are formulated taking into account the radius vectors (54) and (52) which are shown as:

$$h_B = y_o - 4R\cos^2(q_o)\sin(q_o) \tag{65}$$

$$h_O = y_o \tag{66}$$

The mass flow $\dot{m}_R$ is formulated in (Morrell, 1996) and taking into consideration Fig. 3, is obtained

$$\dot{m}_R = \rho_r v_R L dR \tag{67}$$

Consequently, substituting (64)–(67) in (48), $d\dot{W}_I$ is updated as:

$$d\dot{W}_I = 4\rho_r L v_R R g(1 - \sin^2(q_o))\sin(q_o)dR \tag{68}$$

Integrating (68) from R_{min} to $\frac{d_e}{2}$, the impact power on the kidney it is obtained

$$\dot{W}_I = \int_{R_{min}}^{\frac{d_e}{2}} 4\rho_r L v_R R g(1 - \sin^2(q_o))\sin(q_o)dR \tag{69}$$

in which has been considered that the torque applied to the mill τ_L is the necessary and sufficient so that the grinding media falls into the kidney and not into the liners.

The torque τ_η of (44) is responsible for performing the work to move the kidney to the position q_2 overcoming the gravitational forces and the internal frictional forces of the kidney, consequently the net power transmitted to the kidney is determined by:

$$\dot{W} = \tau_\eta \dot{q} \tag{70}$$

To define the abrasion power it is enough to make the difference between the net power and the impact power:

$$\dot{W}_A = \dot{W} - \dot{W}_I \tag{71}$$

The benefit of obtaining the impact power and the abrasion power separately is that it is feasible to relate them to the impact breakage function, the abrasion breakage function, the impact breakage kinetics and the abrasion breakage kinetics, respectively, which will be developed in a future research.

2.8 State Space Model of the Impact and Abrasion Power

In order to obtain a state space model, variables are defined: x_1 as the position q of the mill and x_2 as the position q_2 of the load of the mill:

$$x_1 = q \Rightarrow \dot{x}_1 = \dot{q}, \qquad x_2 = q_2 \Rightarrow \dot{x}_2 = \dot{q}_2$$
$$x_3 = \dot{q} \Rightarrow \dot{x}_3 = \ddot{q}, \qquad x_4 = \dot{q}_2 \Rightarrow \dot{x}_4 = \ddot{q}_2$$

Making algebraic manipulations to (46), (47), (69) and (71), the model is obtained:

$$\begin{bmatrix} \dot{x}_1 \\ \dot{x}_2 \\ \dot{x}_3 \\ \dot{x}_4 \end{bmatrix} = \begin{bmatrix} x_3 \\ x_4 \\ -\mathbf{M^{-1}P}\begin{bmatrix} x_3 \\ x_4 \end{bmatrix} - \mathbf{M^{-1}d} \end{bmatrix} + \begin{bmatrix} \mathbb{0} \\ \mathbb{0} \\ \mathbf{M^{-1}} \end{bmatrix}\mathbf{u} \tag{72}$$

$$\mathbf{y} = \begin{bmatrix} \dot{W}_I(x_1, x_2, x_3, x_4) \\ \dot{W}_A(x_1, x_2, x_3, x_4) \end{bmatrix} \tag{73}$$

where:

$$\mathbf{M} = \begin{bmatrix} M_{11} & 0 \\ 0 & M_{22} \end{bmatrix} \quad \mathbf{P} = \begin{bmatrix} P_{11} & 0 \\ 0 & P_{22} \end{bmatrix} \quad \mathbf{u} = \begin{bmatrix} \tau_L \\ K\dot{q} \end{bmatrix} \quad \mathbf{d} = \begin{bmatrix} d_1 \\ d_2 \end{bmatrix}$$

$$K = \frac{\eta\alpha\left(\frac{d}{2}\right)^3 L}{\frac{d}{2} - R_r} \qquad M_{11} = J_t + \frac{1}{4}d_p^2(m_g + m_c) + \frac{\rho_g V_l d_p^2 s_{q_o}}{4\beta\sqrt{1 - s_{q_o}^2}}$$

$$M_{22} = m_r R_r^2 \qquad P_{11} = B_t + \frac{1}{4}d_p^2\dot{m}_g + \frac{\eta\alpha\left(\frac{d}{2}\right)^3 L}{\frac{d}{2} - R_r}$$

$$P_{22} = \frac{\dot{q}_2}{2}(m_{dr}R_r^2 + 2m_r R_{dr}R_r) + \frac{\eta\alpha\left(\frac{d}{2}\right)^2 R_r L}{\frac{d}{2} - R_r}$$

$$d_1 = -\frac{\eta\alpha\left(\frac{d}{2}\right)^2 R_r L}{\frac{d}{2} - R_r}\dot{q}_2 + \mu m_{r_1} g\frac{d}{2}(-\sin(q_2))$$

$$d_2 = g(m_{dr}R_r + m_r R_{dr})\sin(q_2) + g m_r R_r\cos(q_2) - \mu m_{r_1} g\frac{d}{2}(-\sin(q_2)) \tag{74}$$

3. RESULTS AND EVALUATION

To evaluate the performance of the obtained model, some simulation studies of net power were carried out with a load of 40% for a 15 MW ball mill. In Fig. 4 and Fig. 5 are shown how the impact power and the abrasion power vary each other. Thus, impact power is grater than abrasion power for a torque percentage of 89% and abrasion power is grater than impact power for a torque percentage of 68%. This approach also allows representing other important variables such speed of the mill and the load angle of the kidney for the chosen operating conditions (see Fig. 6).

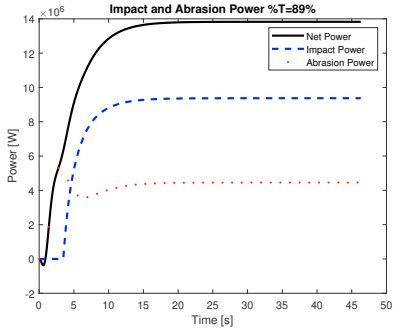

Fig. 4. Impact power vs abrasion power for a torque percentage of 89%.

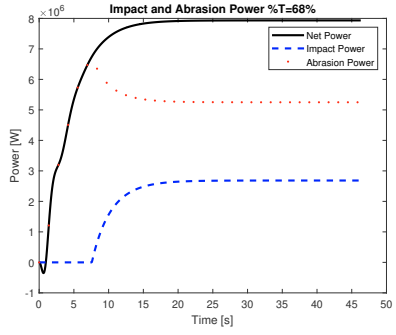

Fig. 5. Impact power vs abrasion power for a torque percentage of 68%.

4. CONCLUSION

A model representing the dynamics of the impact power and the abrasion power separately in a tumbling mill, which together regulate the dynamics of the reduction of the mineral inside the mill was proposed. The proposed model takes the operating conditions of the mill into consideration, which implies that the model is valid throughout a given operating range, it is also represented in the state space, which will facilitate the control design task. Finally, simulation tests were carried out for a tumbling mill. Possible future directions include extension to control design and optimization based on the proposed model.

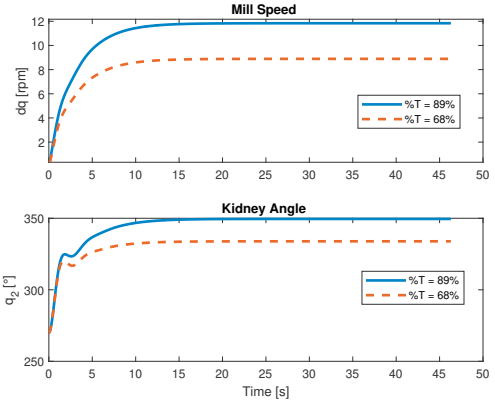

Fig. 6. Mill speed and load angle of the kidney for a torque percentage of 89% and 68%.

ACKNOWLEDGEMENTS

This work was financially supported by CONCYTEC-PROCIENCIA within the framework of the call E070-2021-01, “Movilizaciones para investigación - AmSud” [CONTRATO N° 054-2021-PROCIENCIA].

REFERENCES

Bond, F. (1961). Crushing and grinding calculations. *Allis Chalmers Publication*, 07R9235B.

Herbst, J. and Fuerstenau, D. (1980). Scale-up procedure for continuous grinding mill design using population balance models. *International Journal of Mineral Processing*, 7, 1–31.

Hogg, R. and Fuerstenau, D. (1972). Power relationship for tumbling mills. *Transactions of the Society of Mining Engineers–AIME.*, 252, 418–432.

Jayasundara, C. and Zhu, H. (2022). Impact energy of particles in ball mills based on dem simulations and data-driven approach. *Powder Technology*, 395, 226–234.

le Roux, J.D., Craig, I., Hulbert, D.G., and Hinde, A.L. (2013). Analysis and validation of a run-of-mine ore grinding mill circuit model for process control. *Minerals Engineering.*, 43-44, 121–134.

Morrell, S. (2004). A new autogenous and semi-autogenous mill model for scale-up, design and optimisation. *Minerals Engineering*, 17, 437–445.

Morrell, S. (1996). Power draw of wet tumbling mills and its relationship to charge dynamics - part 1: A continuum approach to mathematical modelling of mill power draw. *Transactions of the Institutions of Mining and Metallurgy, Section C: Mineral Processing and Extractive Metallurgy.*, 105, C43–C51.

Salcedo Hernandez, J., Rivas-Perez, R., and Sotomayor Moriano, J.J. (2018). Design of a generalized predictive controller for temperature control in a cement rotary kiln. *IEEE Latin America Transactions*, 16(4), 1015–1021.

Yuwen, C., Sun, B., and Liu, S. (2020). A dynamic model for a class of semi-autogenous mill systems. *IEEE Access.*, 8, 98460–98470.